2014 44

Resolved Star Formation Surface Density and Stellar Mass Density of Galaxies in the Local Universe

Abdurrouf
Astronomical Institute of Tohoku University

Abstract

In order to understand how the stellar mass are distributed within the galaxies in the local Universe, where the stars are being made in high star formation rate in them, and relation between their morphology and their activities in making stars, we are going to investigate the surface density of star formation rates (SFRs) and stellar mass surface density by analyzing the resolved stellar population properties of 445 massive galaxies at $0.01 < z < 0.02$. The galaxy images will be taken from SDSS DR10. Only galaxies with stellar mass more than $10^{10.5}$ $M_{\odot}$ will be selected. The sample will be differentiated according to their morphology (elliptical, spiral, and irregular) and each galaxy's surface will be divided into inner (center) and outer region. Resolved stellar population properties, that is star formation rate, age, stellar mass, and extinction, will be derived by modelling the spectral energy distribution (SED) for each spatial bin of galaxy image. Then calculation and analysis will be focused on stellar mass density, density of star formation rate, age, and extinction as a function of galactocentric radius.

1 Introduction

It has been known currently that morphology of galaxies (elliptical, spiral, or irregular) is related to their star formation history (SFH). How galaxies were forming their stars in the past seems to affect their future appearance. Elliptical galaxies likely formed all their stars from sudden burst in the past when they was still assembled, so that they are now dominated by red old stars and lack or almost contain no young blue stars. Elliptical galaxies are very luminous and massive system with high mass to light ratio which infer that this galaxies contain many dark matter halo in their outer part. Cold gas is almost not found in the elliptical galaxies, but some of them have very small fraction of cold gas in their central region which might still be the fuel for star formation. Different to elliptical galaxies, spiral galaxies and irregular galaxies are still forming their stars now as they contain many young blue stars. Spiral galaxy which prominent with their spiral pattern and rotational motion of their disk stars, have more young blue stars lying in the spiral arms and disk compare to the central bulge which contains old red stars and has high metallicity. Star forming activities inside galaxy determine by many factors, such as existence of cold gas, and dynamical fluctuation which can triggers gas shrinking due to gravitational contraction. Supernova explosion of dead stars spreads their metals contain and shed surrounding gas which can compress gas in other places and trigger next star birth. Merger or close encounter between two galaxies also can trigger star birth inside each galaxy by the dynamical instability produced by the merger or close encounter process. Frictional motions of orbiting gas make loss of their energy and eventually fall inward sum up the concentration of gas in the central part of galaxy. This might cause the high star formation activities in the central part of galaxy. In order to understand this star formation activity flow inside galaxy, we need to know the distribution of stellar mass density and star formation rate (SFR) surface density of galaxies in local Universe as well as in distant Universe. In order to calculate the distribution of stellar mass density and star formation rate density inside galaxy as well as other stellar population properties, one method that we can used is by fitting the resolved spectral energy distribution (SED) instead of integrated SED of galaxy. Resolved SED fitting have been widely used to study the stellar mass density as well as star formation rate (SFR) and star formation history (SFH) (Conti, A. et al. 2003; Welikala, N. et al. 2008; Welikala, N. et al. 2009; Zibetti, S. et al. 2009; Wuyts, S. et al. 2012; Wuyts, S. et al. 2013). In the resolved SED fitting, multi-wavelength band photometry are calculated for each spatial bin, then stellar population synthesis model is built in such way to fit this photom-

etry SED. Total stellar mass obtained by integrating resolved stellar mass is can be different compare with those obtained by unresolved photometry (Zibetti, S. et al. 2009) which might be caused by effect of dust extinction. Total star formation rate (SFR) and other stellar population properties (age, dust obscuration) obtained from integrating resolved SFR also different compare with those obtained by fitting unresolved photometry (Wuyts, S. et al. 2012). Studying resolved stellar population properties might give clue to more detailed understanding on galaxy structure and evolution processes occurred inside it.

2 Methods/Instruments and Observations

2.1 Data Sample

In this research we will use optical data from SDSS Data Release 10 for massive galaxies (M > $10^{10.5}$M$_\odot$ lying in redshift range of 0.01 < z < 0.02. SDSS is providing five-band broad band photometry (ugriz bands), and the spectroscopic follow-up of most galaxies. In additional to the data product of SDSS, we use value-added MPA/JHU DR7 galaxy catalogs. These catalogs contain information about total stellar mass (based on Kauffman et al. 2003 and Salim et al. 2007) and star formation rate (based on Brinchmann et al. 2004) of 927552 galaxies of SDSS data. Location of our sample with respect to overall galaxies more massive than 10^6 M$_\odot$ lying in redshift range of 0.01 <z <0.02 can be seen from Figure 1.

2.2 PSF Matching

Before performing resolved SED fitting to galaxy image, we need to match the point-spread function among five band images of all 445 galaxies. PSF matching is done by matching the average FWHM (full width in half maximum) of PSF profile of foreground stars (which appears in the image) with reference value of FWHM. Reference value for FWHM is taken from image band which has highest average value of FWHM. For matching FWHM we use Gaussian convolution in IRAF (gauss command). For calculating FWHM we use SExtractor (Bertin Arnouts 1996). SExtractor work by detecting the objects (stars and galaxies) inside the image field (which might can't be seen by our eye) then calculate the parameter/physical properties (of those detected objects) which we want to calculate (selecting it from default parameter list provided by SExtractor). In our case, we calculate magnitude and FWHM of each detected object. Following figure shows one example of PSF matching resulted for one band. FWHM value is increased after been convolved as we can see from Figure 2.

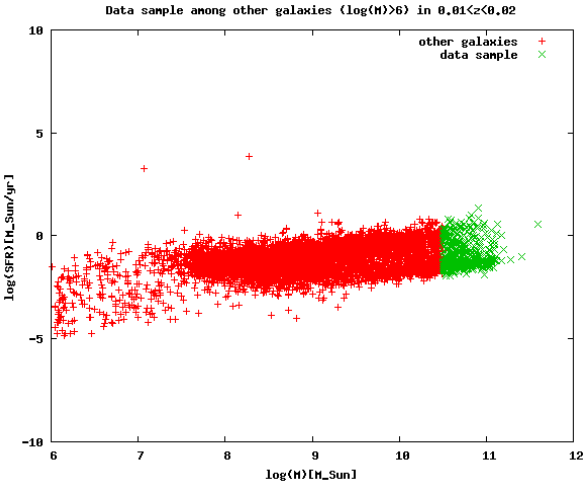

1: Location of data sample among galaxies more massive than 10^6 M$_\odot$ which lie in 0.01 < z < 0.02

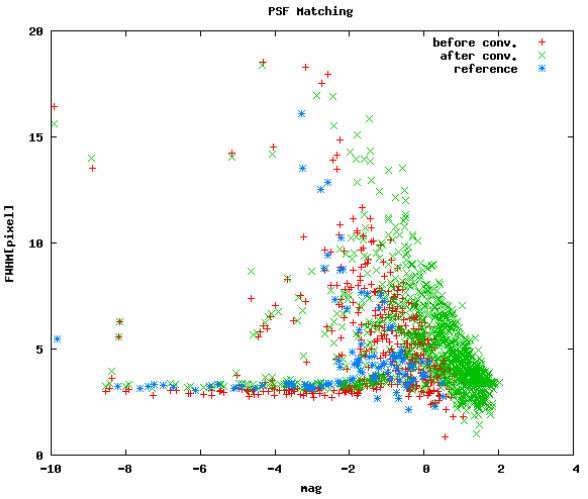

2: Comparison between FWHM value before and after being Gaussian convolved

2.3 Pixel Binning

For assigning pixels to objects, we use the SExtractor (Bertin Arnouts 1996) segmentation map. We group pixel adopt the Voronoi two-dimensional binning technique (Cappellari Copin 2003), instead of apply multi-wavelength photometric for each pixel individually.

2.4 Resolved SED Fitting

First we perform standard stellar population modelling of five bands (ugriz) of each spatial bin individually. That is, we fit Bruzual Charlot (2003) model to the five bands (u-to-z) and search for the least-squares solution using the fitting code FAST (Kriek et al. 2009). Some constraints we use in this modelling are : range of age between 50 Myr (onset of star formation) and the age of the Universe, visual extinctions in the range $0 < A_V < 4$ with reddening following Calzetti et al. (2000), and SFHs which decline with -folding times down to Myr. For initial mass function (IMF), we adopt a Chabrier (2003) model.

3 Results

Until now, 10 galaxy images have been downloaded from SDSS DR 10 and PSF matched, value-added MPA/JHU DR7 galaxy catalogs have been downloaded. But neither these 10 galaxies nor 435 others haven‘t been SED fitted. So in this proceeding we only show our current result, that is PSF matching of 10 galaxies which can be seen from Figure 3 (in Appendix).

Acknowledgement

Funding for the Sloan Digital Sky Survey IV has been provided by the Alfred P. Sloan Foundation and the Participating Institutions. SDSS-IV acknowledges support and resources from the Center for High-Performance Computing at the University of Utah. The SDSS web site is www.sdss.org. SDSS-IV is managed by the Astrophysical Research Consortium for the Participating Institutions of the SDSS Collaboration including the Carnegie Institution for Science, Carnegie Mellon University, the Chilean Participation Group, Harvard-Smithsonian Center for Astrophysics, Instituto de Astrofsica de Canarias, The Johns Hopkins University, Kavli Institute for the Physics and Mathematics of the Universe (IPMU) / University of Tokyo, Lawrence Berkeley National Laboratory, Leibniz Institut fr Astrophysik Potsdam (AIP), Max-Planck-Institut fr Astrophysik (MPA Garching), Max-Planck-Institut fr Extraterrestrische Physik (MPE), Max-Planck-Institut fr Astronomie (MPIA Heidelberg), National Astronomical Observatory of China, New Mexico State University, New York University, The Ohio State University, Pennsylvania State University, Shanghai Astronomical Observatory, United Kingdom Participation Group, Universidad Nacional Autnoma de Mxico, University of Arizona, University of Colorado Boulder, University of Portsmouth, University of Utah, University of Washington, University of Wisconsin, Vanderbilt University, and Yale University.

Reference

Bertin, E., Arnouts, S. 1996, Astronomy Astrophysics Supplement Series, 117, 393
Brinchmann, J., Charlot, S., White, S. D. M. 2004, MNRAS, 351, 1151
Bruzual, G., Charlot, S. 2003, MNRAS, 344, 1000
Calzetti, D., Armus, L., Bohlin, R. C., et al. 2000, The Astrophysical Journal, 533, 682
Capellari, M., Copin, Y. 2003, MNRAS, 342, 345
Chabrier, G. 2003, PASP, 115, 763
Conti, A., et al. 2003, The Astronomical Journal, 126, 2330
Kauffmann, G., et al. 2003, MNRAS, 341, 33
Kriek, M., van Dokkum, P. G., Labbe, I., et al. 2009, The Astrophysical Journal, 700, 221
Salim, S., et al. 2007, The Astrophysical Journal Supplement Series, 173, 267
Welikala, N., Connolly, A. J., Hopkins, A. M., Scranton, R., Conti, A. 2008, The Astrophysical Journal, 677, 970
Welikala, N., Connolly, A. J., Hopkins, A. M., Scranton, R. 2009, The Astrophysical Journal, 701,994
Wuyts, S., et al. 2012, The Astrophysical Journal, 753, 114
Wuyts, S., et al. 2013, The Astrophysical Journal, 779, 135
Zibetti, S., Charlot, S., Rix, H. W. 2009, MNRAS, 000, 1

Appendix

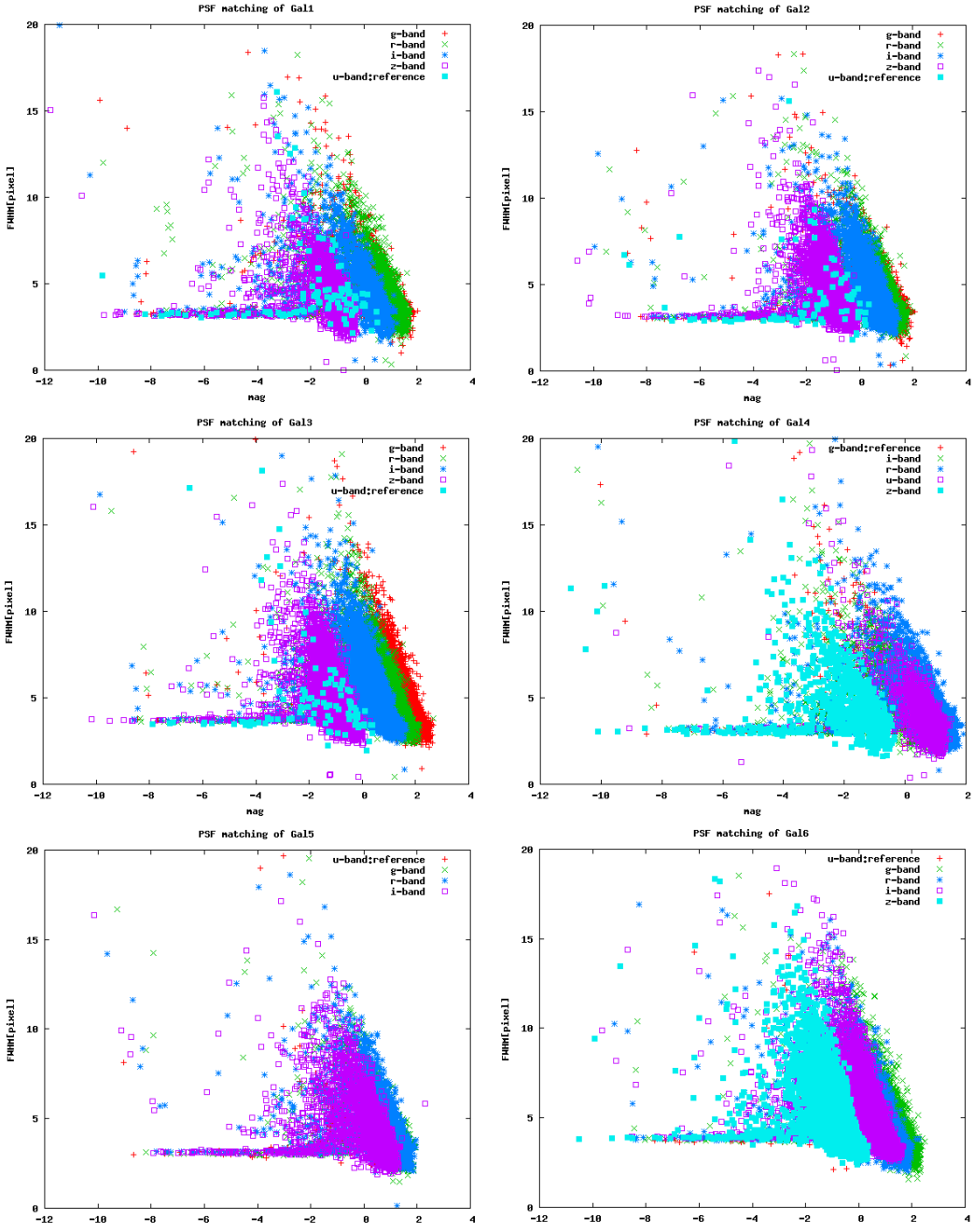
PSF matching of Gal1
g-band
r-band
i-band
z-band
u-band;reference
FWHM[pixel]
mag
PSF matching of Gal2
g-band
r-band
i-band
z-band
u-band;reference
FWHM[pixel]
mag
PSF matching of Gal3
g-band
r-band
i-band
z-band
u-band;reference
FWHM[pixel]
mag
PSF matching of Gal4
g-band;reference
i-band
r-band
u-band
z-band
FWHM[pixel]
mag
PSF matching of Gal5
u-band;reference
g-band
r-band
i-band
FWHM[pixel]
PSF matching of Gal6
u-band;reference
g-band
r-band
i-band
z-band
FWHM[pixel]

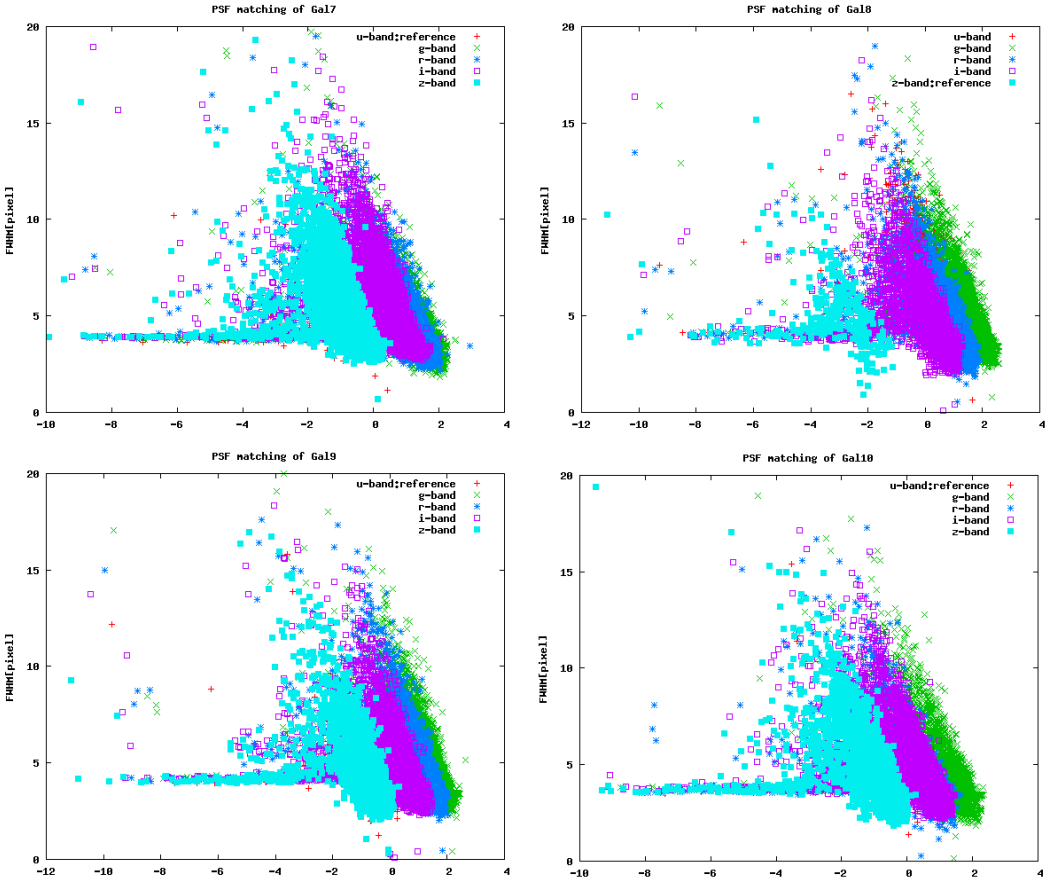

3: PSF Matching result for 10 galaxies